Acta Crystallographica Section D
Biological Crystallography
ISSN 0907-4449

Expansion of the aspartate β-semialdehyde dehydrogenase family: the first structure of a fungal ortholog

Buenafe T. Arachea, Xuying Liu,‡ Alexander G. Pavlovsky and Ronald E. Viola*

Department of Chemistry, University of Toledo, Toledo, Ohio 43606, USA

‡ Present address: Yale University School of Medicine, Department of Pharmacology, New Haven, CT 06520, USA.

Correspondence e-mail: ron.viola@utoledo.edu

Received 8 October 2009
Accepted 8 December 2009

PDB Reference: caASADH, 3hsk.

The enzyme aspartate semialdehyde dehydrogenase (ASADH) catalyzes a critical transformation that produces the first branch-point intermediate in an essential microbial amino-acid biosynthetic pathway. The first structure of an ASADH isolated from a fungal species (*Candida albicans*) has been determined as a complex with its pyridine nucleotide cofactor. This enzyme is a functional dimer, with a similar overall fold and domain organization to the structurally characterized bacterial ASADHs. However, there are differences in the secondary-structural elements and in cofactor binding that are likely to cause the lower catalytic efficiency of this fungal enzyme. Alterations in the dimer interface, through deletion of a helical subdomain and replacement of amino acids that participate in a hydrogen-bonding network, interrupt the intersubunit-communication channels required to support an alternating-site catalytic mechanism. The detailed functional information derived from this new structure will allow an assessment of ASADH as a possible target for antifungal drug development.

1. Introduction

The aspartate pathway for amino-acid biosynthesis is essential for the viability of most microorganisms (Gerdes *et al.*, 2003; Kobayashi *et al.*, 2003; Thanassi *et al.*, 2002). In addition to serving as the source of four of the amino acids required for protein synthesis (Viola, 2001), this pathway produces several metabolites that play crucial roles in various cellular functions. These include the precursors for cell-well cross-linking (diaminopimelate) (van Heijenoort, 2001), for sporulation in certain Gram-positive bacteria (dipicolinate) (Ragkousi *et al.*, 2003), for methylation reactions (*S*-adenoylmethionine) and for quorum sensing in Gram-negative bacteria (homoserine lactone) (Lyon & Novick, 2004). The commitment step to this pathway involves the phosphorylation of aspartic acid, which is catalyzed by multiple aspartokinases in most organisms (Cohen, 1985). These enzymes are frequently under allosteric control by the end-product amino acids and can also be bifunctional, containing an additional catalytic domain. The second reaction in this pathway, which is catalyzed by aspartate β-semialdehyde dehydrogenase (ASADH), produces the first branch-point metabolite and is a critical bottleneck in the flux through the pathway.

ASADH has been mechanistically characterized (Karsten & Viola, 1991) and representative structures have been determined from Gram-negative (Blanco *et al.*, 2003; Hadfield *et al.*, 2001), Gram-positive (Faehnle *et al.*, 2006) and archaeal

species (Faehnle *et al.*, 2005). Based on this structural and mechanistic background, a series of selective inhibitors are being investigated as potential lead compounds for the production of new antibacterial agents. However, to date no structural information has been obtained on any ASADHs from fungal sources in order to guide the development of antifungal agents.

ASADH from the yeast *Candida albicans* (*ca*ASADH) has been cloned and purified and its structure has now been determined to moderately high resolution in the presence of its nucleotide cofactor. Comparison of this new structure with the existing family of ASADH structures has identified a number of similarities, as well as some critical differences, that will guide future inhibitor design and development.

Table 1
Data-collection statistics for the *ca*ASADH–NADP complex.

Values in parentheses are for the highest resolution shell.

Temperature (K)	100
Space group	$C222_1$
Unit-cell parameters (Å, °)	a = 93.41, b = 152.18, c = 97.76, $\alpha = \beta = \gamma = 90$
Wavelength (Å)	1.033
Resolution (Å)	2.2 (2.3–2.2)
Total reflections	162700
Unique reflections	32749
Mosaicity (°)	0.94
$R_{\rm merge}$	0.077 (0.44)
Output $\langle I/\sigma(I)\rangle$	20.2 (2.0)
Completeness (%)	91.5 (60.6)
Redundancy	5.1 (2.3)

2. Materials and methods

2.1. Cloning, expression and purification of *ca*ASADH

The *hom2* gene encoding aspartate β-semialdehyde dehydrogenase was amplified from *C. albicans* genomic DNA using standard polymerase chain reaction methods. The amplified gene was ligated into pET-28 expression vector containing an N-terminal hexahistidine tag using *Nde*I/*Eco*RI endonuclease restriction sites to yield the *ca*ASADH plasmid. The plasmid was transformed into *Escherichia coli* strain BL21 cells and grown at 310 K in 2 l flasks containing Luria broth medium supplemented with 30 µg ml^{-1} kanamycin. Protein expression was initiated by the addition of 1 m*M* IPTG and the temperature was lowered to 301 K and maintained for 5 h, after which the cells were recovered by centrifugation.

Cells were resuspended in 50 m*M* Tris–HCl pH 7.5, 2 m*M* β-mercaptoethanol and 200 m*M* ammonium acetate and lysed by ultrasonication followed by centrifugation to obtain a soluble fraction. The soluble fraction was loaded onto a cobalt immobilized metal-affinity (IMAC) column and the target enzyme was eluted using an imidazole gradient from 0 to 200 m*M*. Further purification was carried out with a high-resolution anion-exchange column (Source 30Q) pre-equilibrated with 40 m*M* MES pH 6.5, 1 m*M* EDTA and 2 m*M* DTT. The *ca*ASADH enzyme was separated from remaining impurities using an ammonium acetate gradient (0–500 m*M*). The enzyme was assessed to be >95% pure based on SDS–PAGE profiles and was shown by dynamic light scattering (DLS) to exhibit <10% polydispersity, which is indicative of a highly purified homogeneous protein. The protein was dialyzed into storage buffer (20 m*M* HEPES pH 7.0, 2 m*M* DTT and 1 m*M* EDTA) and was concentrated to 20 mg ml^{-1} for crystallization using an Amicon spin concentrator (10 kDa molecular-weight cutoff).

2.2. Crystallization

Initial screening of crystallization conditions for the apo form of *ca*ASADH was carried out with various commercial screening kits as well as with in-house custom screens, each of which gave several crystallization hits. After extensive optimization of the preliminary crystallization conditions, rod-shaped crystals of the apoenzyme were obtained with 16 mg ml^{-1} protein, 16–18% PEG 2000 monomethyl ether, 0.1 *M* MES pH 6.5, 0.1 *M* NaCl and 0.1 *M* Li_2SO_4 at 293 K using the hanging-drop vapor-diffusion method. These crystals diffracted to 2.7 Å resolution but with very high mosaicity. The diffraction patterns indicated the presence of multiple crystals in the sample, thus making it difficult to obtain a useable solution for the apoenzyme structure.

Because of the difficulty in obtaining high-quality apoenzyme crystals, efforts were focused on obtaining diffraction-quality crystals of the *ca*ASADH–NADP complex. This binary complex was prepared using a final protein concentration of 10 mg ml^{-1} in the presence of 2 m*M* NADP. Several initial crystallization conditions were identified from the PEG/Ion Screen (Hampton Research). Improved clusters of rod-shaped crystals were obtained from drops grown in 20% PEG 400 and 0.1 *M* HEPES pH 6.5. After further optimization by varying the protein concentration as well as by screening different additives, single crystals grew from a 1:1 mixture of the complex solution (14 mg ml^{-1} protein, 2 m*M* NADP) and reservoir solution (20% PEG 400, 0.1 *M* HEPES pH 6.5, 0.1 *M* $MgCl_2$) after several days of incubation at 293 K. Crystals were harvested and subsequently transferred to a cryogenic solution prepared from the reservoir solution and 25% glycerol, after which the cryoprotected crystal was flash-frozen in liquid nitrogen for data collection.

2.3. Data collection and processing

Preliminary screening of the diffraction quality of the crystals was conducted in-house with a Rigaku FR-E rotating-anode generator equipped with an R-AXIS IV image-plate detector. Subsequent synchrotron X-ray diffraction data for the NADP complex were collected on the GM-CAT Sector 23B beamline at the Advanced Photon Source (Argonne National Laboratory). A complete data set was collected from a single frozen crystal of the NADP complex. The images were processed using *HKL*-2000 (Otwinowski & Minor, 1997) and scaling of the data set was performed with the *SCALEPACK* program. The data-collection statistics for the NADP complex are summarized in Table 1. The crystal belonged to the orthorhombic space group $C222_1$ with the asymmetric unit

consisting of two monomers, giving a Matthews coefficient of 2.13 Å^3 Da^{-1} and a solvent content of ∼42%.

2.4. Structure determination, refinement and validation

The structure of the binary complex was solved by molecular replacement using the program *Phaser* (McCoy *et al.*, 2005) and a monomer of the archeal ortholog of ASADH from *Methanococcus jannaschii* (*mj*ASADH; PDB code 1ys4; Faehnle *et al.*, 2005). Sequence comparison of the *ca*ASADH enzyme with various ASADHs indicated that *mj*ASADH has 60% sequence similarity and 40% sequence identity to this fungal ASADH. The data from 79 to 3.5 Å resolution were utilized in the initial search and a molecular-replacement solution was obtained with a final TFZ score of 14. The resulting model was then subjected to 20 cycles of rigid-body refinement using the medium-resolution data to 3.5 Å. This refinement gave an initial *R* value of 0.51. The model was further refined using the *REFMAC* program (Winn *et al.*, 2001) and restrained refinement from 79 to 2.2 Å resolution, thereby lowering the *R* value to 0.40. The structure of the *ca*ASADH–NADP complex was built by a combination of manual building in *Coot* (Emsley & Cowtan, 2004) followed by iterative rounds of restrained refinement. Validation of the structure was carried out using *PROCHECK* from the *CCP*4 suite (Collaborative Computational Project, 1994). Surface calculations were conducted using *PISA* (*Protein Interfaces, Surfaces and Assemblies*; http://www.ebi.ac.uk/msd-srv/prot_int/pistart.html).

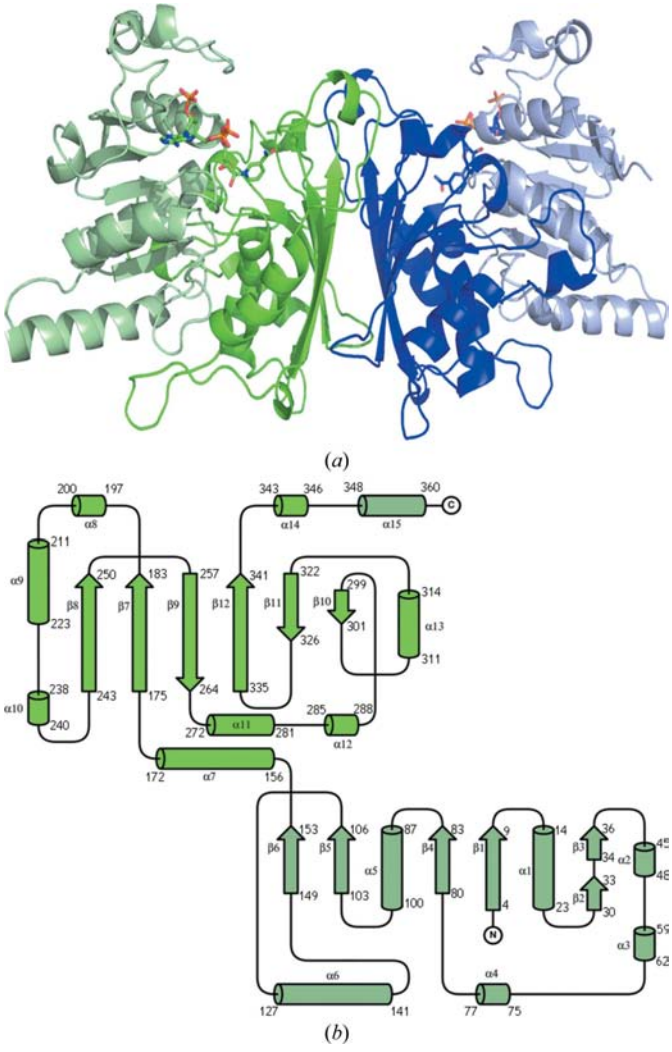

Figure 1
Overall structure of the fungal ASADH enzyme from *C. albicans* complexed with NADP (PDB code 3hsk). (*a*) The two monomeric units are colored green and blue. The amino-terminal coenzyme-binding domains (residues 2–155 and 347–365) are colored in lighter shades and the carboxyl-terminal catalytic and dimerization domains (residues 155–346) in darker shades. (*b*) Topology map showing the organization of the secondary structure of *ca*ASADH.

Table 2
Refinement statistics for the *ca*ASADH–NADP complex.

Values in parentheses are for the highest resolution shell.

Resolution range (Å)	79–2.2 (2.3–2.2)
Wilson *B* factor (Å^2)	42.4
No. of reflections	32667
R_{work}/R_{free} (%)	0.23/0.28 (0.28/0.37)
R.m.s.d. bonds (Å)	0.007
R.m.s.d. angles (°)	1.115
No. of molecules per ASU	2
No. of atoms	
Protein	5350
Ligands	48
Waters	147
B factors (Å^2)	
Protein	48
Ligands	82
Waters	49
Ramachandran plot analysis (%)	
Most favored	93.6
Additionally allowed	6.4
Generously allowed	0
Disallowed	0

3. Results and discussion

3.1. Structural refinement

The structure of the *ca*ASADH–NADP complex was solved using the molecular-replacement program *Phaser*, utilizing the monomer of the most homologous ASADH enzyme from *M. janaschii* as the search model. A series of manual building and cycles of iterative restrained refinement with the data resolution extended to 2.2 Å produced the final structure of the binary complex with refinement values R_{work} and R_{free} of 0.23 and 0.28, respectively. The refinement statistics for this complex structure are summarized in Table 2.

The final electron-density map allowed complete building of residues 2–187 and 194–365 for each monomer, with both monomers lacking interpretable density for residues 188–193. However, seven residues in monomer *A* and nine residues in monomer *B* were modeled as alanines owing to lack of density to fully model the side chains. The truncated residues are primarily surface amino acids with long side chains such as lysine and arginine.

3.2. Overall structure of the *ca*ASADH–cofactor complex

The asymmetric unit of the *ca*ASADH–NADP complex contains two subunits that represent the functional homodimer of this enzyme. As has been observed for other members of the ASADH structural family, each monomeric unit is composed of an N-terminal coenzyme-binding domain (residues 2–155 and 347–365) and a C-terminal catalytic and dimerization domain (residues 156–346) (Fig. 1*a*). The coenzyme-binding domain is made up of six β-strands and seven α-helical segments, while the C-terminal domain consists of six β-strands and eight α-helices that represent the catalytic site and the dimerization interface (Fig. 1*b*). The two monomers are nearly identical in structure, with a backbone r.m.s.d. of 0.4 Å. This fungal ortholog of ASADH most closely resembles the structure of the archeal *mj*ASADH, but with some important structural differences.

3.3. Secondary-structure comparison

The N-terminus of the fungal ASADH starts with a β-strand (β1) followed by an α-helix (α1) connected to two short β-strands (β2 and β3), completing the first β-α-β motif of the Rossmann fold (Fig. 1*b*). The two short β-strands in *ca*ASADH replace the single β-strand that is typically seen in bacterial ASADH structures (Blanco *et al.*, 2003; Faehnle *et al.*, 2006). This motif is then linked to a 44-residue surface loop (residues 36–79) composed of three short helices (α2, α3 and α4) that help to enclose the coenzyme-binding domain. This longer surface loop observed in the fungal enzyme is the result of a ten-residue insert from Gly42 to Trp51 (Fig. 2); this insert include three lysines and an aspartic acid residue that form hydrogen bonds to the peptide backbone of adjacent amino acids.

Following the surface loop in *ca*ASADH is a second β-α-β motif (β4-α5-β5) that is highly conserved among all ASADHs. The ASADH enzyme family also contains a third β-α-β motif, but the primary sequence and architecture of this motif is less conserved among enzymes from different organisms. The fungal enzyme resembles the enzyme from the Gram-positive bacterium *Streptococcus pneumonia* (*sp*ASADH; Faehnle *et al.*, 2006) with respect to the general fold of this third motif, with both enzymes containing an unstructured loop instead of the first β-strand, followed by an α-helix (α6) and a short loop leading to the second β-strand (β6) in the motif (Fig. 1*b*). However, *ca*ASADH features a slightly longer unstructured loop than *sp*ASADH, containing four additional residues, as well as a longer α-helix (α6) composed of residues 127–141 (Fig. 1*b*).

The placement of the active-site nucleophile in *ca*ASADH is also different compared with its position in the bacterial ASADH structures. In the bacterial enzymes this catalytic cysteine is located at the top of a conserved helix (Blanco *et al.*, 2003), while in the fungal structure the end of β7 connects to a short loop that contains the catalytic nucleophile. This location of Cys156 in *ca*ASADH appears to introduce sufficient flexibility to allow an alternative conformation for this

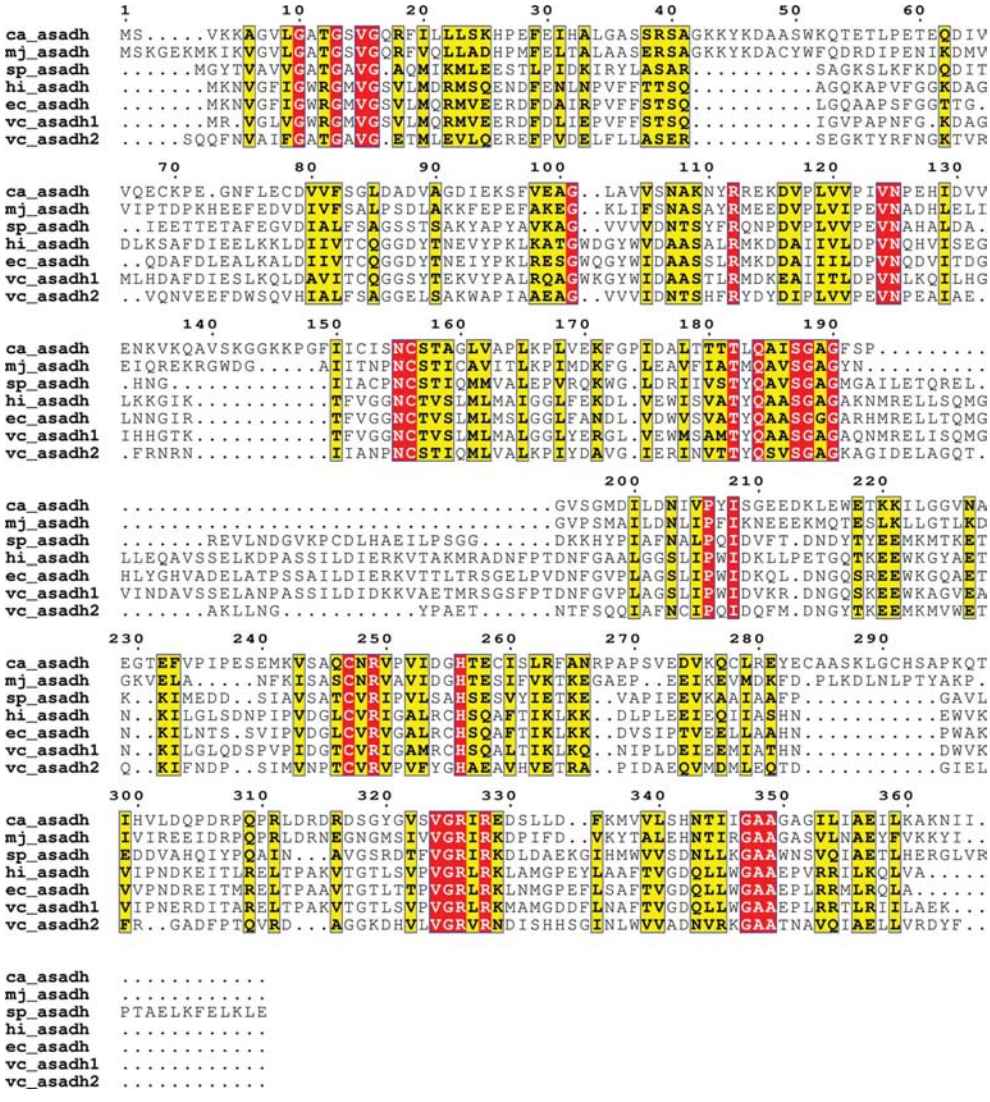

Figure 2
Sequence alignment of representative ASADH enzymes from different archaeal and bacterial species, showing the inserts and deletions between *ca*ASADH and the other enzymes in this family. Fully conserved residues are shown in red boxes and residues with conservative mutations are shown in yellow boxes.

active-site nucleophile (Fig. 3). After this region the loop connects to a conserved helix (α7) and is then directed towards the first β-strand (β7) of the dimerization domain.

Another significant difference in the structure of the fungal enzyme is a missing α-helical subdomain in *ca*ASADH that is part of the dimerization interface in the bacterial ASADHs and reaches across to the coenzyme-binding domain of the adjacent subunit. In the Gram-negative bacteria this helical subdomain is composed of 44 amino acids that are organized in a helix–turn–helix, while this region is somewhat shorter (22–30 amino acids) in the ASADHs from Gram-positive bacteria (Fig. 2). In contrast, this region contains only three residues in *ca*ASADH and, despite being part of a conserved sequence in the ASADH family, there is no interpretable density in this region. These residues are likely to be part of a surface-exposed loop that is observed in *mj*ASADH stretching from residues 184 to 209 (Faehnle *et al.*, 2005). The remainder of the dimerization domain in *ca*ASADH has a similar overall fold to the other ASADH enzymes, but with some critical differences in the length of each β-strand, the presence of intervening short helices and insertions (such as Cys284–Ala294) in the surface loops (Fig. 2) and changes in the identity of key amino acids that provide a communication channel between subunits in the bacterial enzymes.

3.4. Active-site comparison

The functionally important residues that are present in the active site of ASADHs are conserved throughout the entire enzyme family. Superimposition of the residues in the active site of the fungal ASADH with the bacterial *sp*ASADH shows that these conserved residues are each in the same position, except for the active-site cysteine nucleophile, which is found to partially occupy a unique alternative conformation (Fig. 3). The distance from the S atom of Cys156 to the N^{δ} atom of the base catalyst His256 in the likely productive conformation is 3.25 Å, which is similar to the distances observed in the Gram-positive *sp*ASADH (3.22 Å) and the Gram-negative enzyme from *Vibrio cholerae* (*vc*ASADH; 3.1 Å). In the alternative

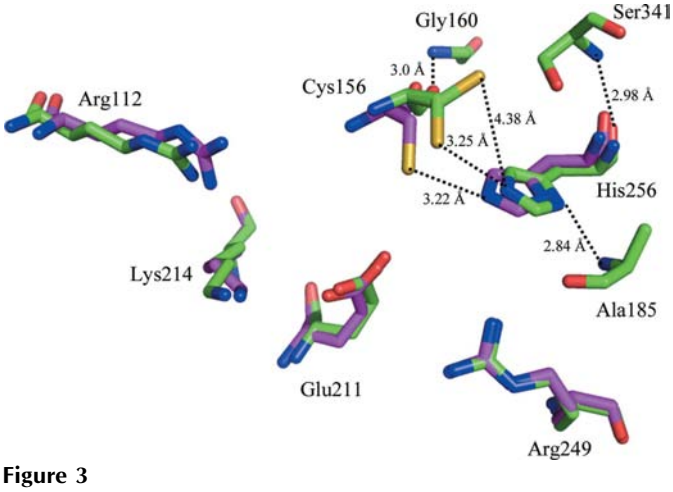

Figure 3
The active site of the fungal ASADH (green), showing the residues involved in substrate binding and catalysis, superimposed with the active-site residues of the bacterial ASADH from *S. pneumonia* (in red). Alternative conformations are seen for the active-site Cys156 nucleophile in *ca*ASADH, with one orientation in a productive interaction (3.25 Å) with the acid–base catalyst (His256) and the other orientation displaced by more than 1 Å.

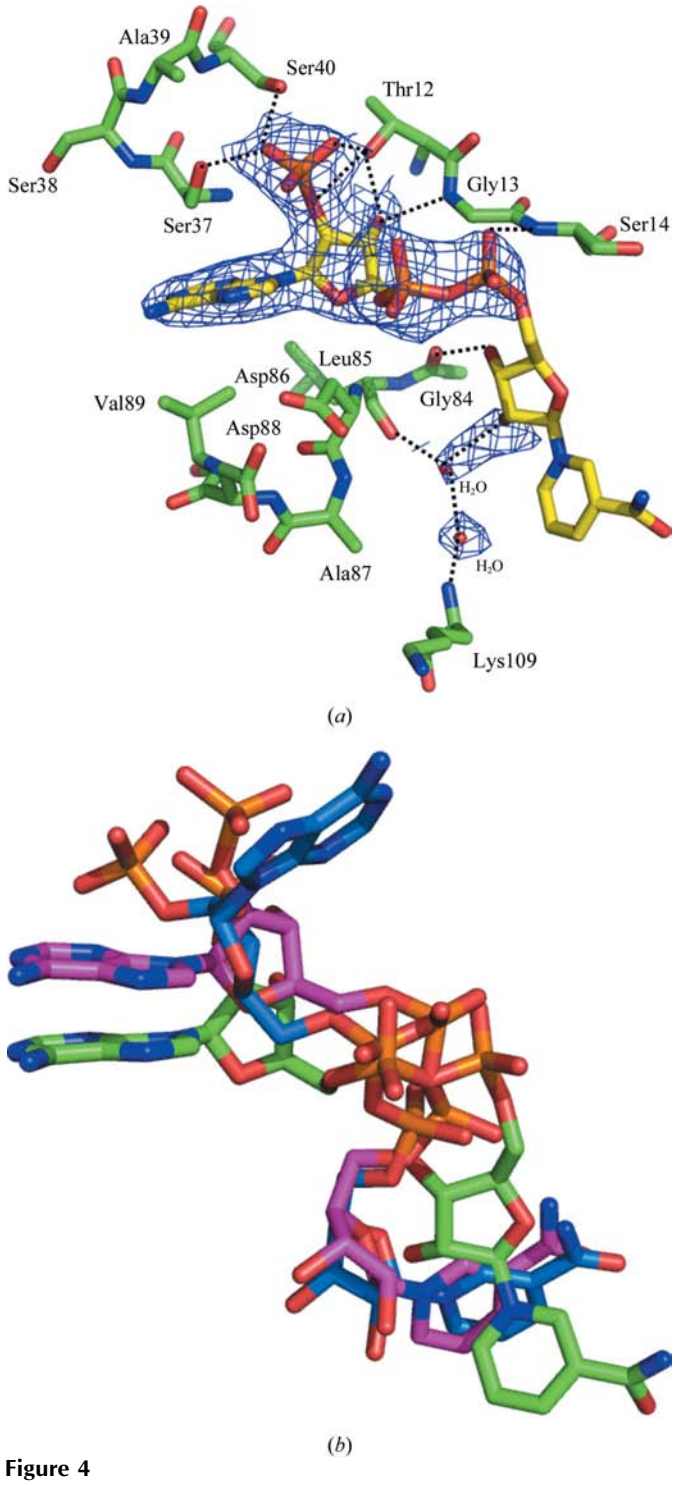

Figure 4
The NADP-binding site in the ASADH enzyme family. (*a*) NADP bound in *ca*ASADH and the residues involved in the cofactor-binding domain. A $2F_o - F_c$ OMIT map of this region contoured at 1σ shows good electron density for the AMP portion of the NADP cofactor but little density for the NMN portion. (*b*) Comparison of the conformations of NADP bound in the ASADH structures from *C. albicans* (green), *S. pneumonia* (red) and *V. cholerae* (blue).

conformation the sulfur-to-nitrogen distance in *ca*ASADH increases to 4.38 Å (Fig. 3) and the position of His256 shifts in response to the changes in the cysteine conformation. A much lower catalytic efficiency would be expected for *ca*ASADH when the active-site cysteine is in this alternative conformation. The position of the catalytic cysteine is stabilized by a hydrogen-bonding interaction of its backbone carbonyl with the amide N atom of Gly160, while the position of His256 is stabilized by a hydrogen bond between its N^{δ} atom and the amide N atom of Ala185, as well as a hydrogen bond between its backbone carbonyl O atom and the amide N atom of Ser341. The remaining active-site residues, including Arg112 and Lys214 which participate in the positioning of the phosphate group and Glu211 and Arg249 which are involved in the binding of aspartate semialdehyde, are all found in the same position as in the bacterial ASADH structures (Fig. 3) and almost certainly play the same roles in the catalytic cycle of these enzymes.

3.5. Differences in cofactor binding

The enzyme *ca*ASADH was crystallized in the presence of its nucleotide cofactor, but differences in the interpretable electron density for the cofactor were observed between the two subunits. One subunit showed continuous density that allowed modeling of the adenine ring as well as one of the phosphates that comprised the diphosphate moiety (Fig. 4*a*), whereas the other subunit contained only broken density in this binding pocket. Neither subunit exhibited complete density for the nicotinamide ring, so the remainder of the NADP molecule was modeled into the structure using the NADP complex structure from the closest ASADH homolog, *mj*ASADH, as a template.

Examination of the network of interactions between NADP and the amino acids in the coenzyme-binding site revealed some similarities and some differences compared with the other ASADHs. The NADP in the *ca*ASADH structure is positioned through interactions with three sets of amino acids, Ser37–Ser40, Thr12–Ser14 and Gly84–Val89, that are located in three different unstructured loops. The hydroxyl side chains of Ser37, Ser40 and Thr12 form hydrogen bonds to the 2′-phosphate group of NADP (Fig. 4*a*). In *sp*ASADH the related side-chain functional groups form the same interactions. However, in the Gram-negative ASADHs the positions of the serine hydroxyl groups are altered and Thr12 is replaced by an arginine. Despite these differences, the 2′-phosphate group is found in nearly the same position in all of the ASADHs.

A more dramatic difference is seen in the positioning of the adenine ring into a completely different pocket in the Gram-negative and Gram-positive bacterial enzymes (Fig. 4*b*). In the enzymes from Gram-negative bacteria Arg9 establishes a cation–π interaction with the adenine ring in *vc*ASADH (Blanco *et al.*, 2003; Viola *et al.*, 2008), while the same residue (Arg10) forms a similar contact with NADP in *ec*ASADH (Hadfield *et al.*, 2001). In addition, there is a hydrogen bond between the 6-amino group of the adenine and the backbone carbonyl of Pro193 that is located in the other subunit of the dimer. In *sp*ASADH the adenine portion of the cofactor is anchored by the interactions of the Ser37 and Thr76 side chains as well as the formation of the cation–π interaction, but now with Arg39. Making these new interactions requires a rotation in the positions of both the adenine and ribose rings, leading to a displacement of as much as 14 Å (Faehnle *et al.*, 2006) when compared with their positions in the Gram-negative enzymes. The adenine moiety in the *ca*ASADH structure is positioned similarly to that observed in the Gram-positive enzyme (Fig. 4*b*), but differences in the identities of the amino acids in this binding pocket alter the nature of the interactions. The adenine ring in *ca*ASADH is sandwiched between residues Ser37, Ser38 and a loop from Gly84 to Val89 (Fig. 4*a*). Residues Asp86–Val89 are too far away to form direct interactions with the adenine ring. The arginine at position 39 in *ca*ASADH is likely to form the same cation–π interaction as observed in *sp*ASADH; however, the electron density in this new fungal structure is not sufficient to orient the arginine side chain and this residue has been truncated to an alanine in this model.

The binding of the remainder of the NADP molecule includes an electro-

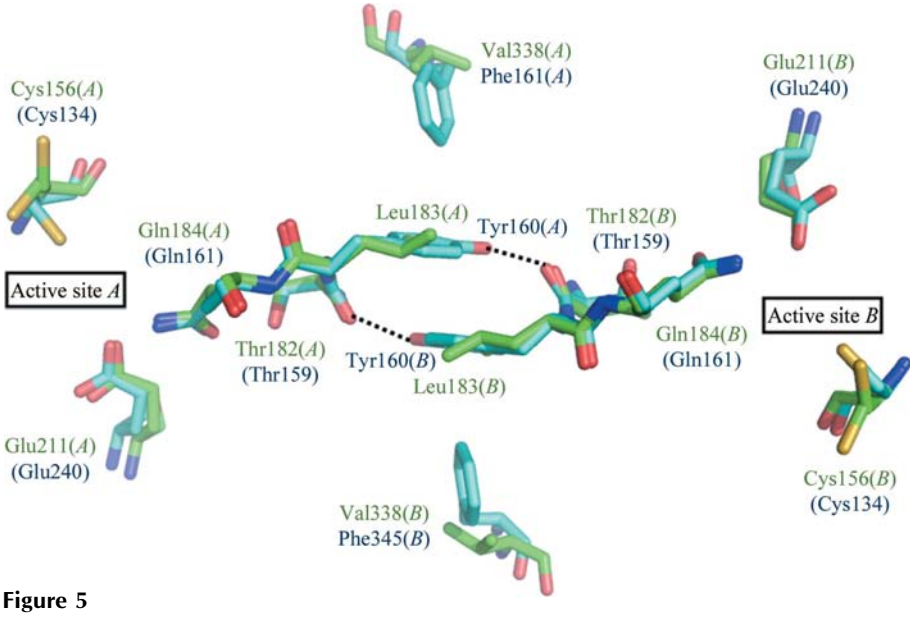

Figure 5
The amino acids that participate in an intersubunit-communication channel between the active sites in each subunit in the Gram-negative bacterial enzymes, represented by the *V. cholerae* ASADH structure, are shown in blue, with the twofold axis perpendicular to the plane of the figure. Replacement of the critical amino acids involved in the hydrogen-bonding network (Tyr160) and the π-stacking stabilization (Phe345) in *ca*ASADH (shown in green) disrupts this communication channel.

static interaction between the pyrophosphate moiety and the backbone amide N atom of Ser14. The 2′-hydroxyl group of the nicotinamide ribose forms hydrogen bonds to a water molecule, which is further stabilized through hydrogen bonds to the carbonyl O atom of Leu85 and an adjacent water molecule. The ribose 3′-hydroxyl group interacts with the carbonyl O atom of Gly84.

3.6. Intersubunit communication

A network of hydrogen-bonding interactions in the dimerization interface of bacterial ASADHs have been proposed to play a key role in intersubunit communication (Blanco *et al.*, 2003). Four amino acids have been identified to be involved in the information-relay process between the active sites in subunits *A* and *B*. In *vc*ASADH the carboxylate side chain of Glu240 in the active site forms a hydrogen bond to the nearby amide side chain of Gln161, which is also hydrogen bonded to the hydroxyl group of Thr159 (Fig. 5). The backbone carbonyl of Thr159 extends this network by forming a hydrogen bond across the dimer interface to the hydroxyl group of Tyr160 from the adjacent subunit. The complementary network of hydrogen-bonding interactions links the active-site Glu240 from subunit *B* to Tyr160 of subunit *A*. The position of these bridging tyrosines is stabilized by π-stacking and by additional perpendicular π-stacking interactions with phenylalanines (Phe345) from their respective subunits (Blanco *et al.*, 2003). This linking four-amino-acid bridge between the active sites of the functional dimer is also observed in a Gram-positive ASADH, with the network of hydrogen-bonding interactions from glutamic acid to tyrosine being conserved in *sp*ASADH (Faehnle *et al.*, 2006). The only difference between *vc*ASADH and *sp*ASADH in this region is the replacement of the phenylalanine in *vc*ASADH with a tryptophan in *sp*ASADH that preserves the stabilizing π-stacking interaction.

The *ca*ASADH enzyme also displayed hydrogen-bonding interactions between the active-site Asp211 and Asn184, which in turn forms a hydrogen bond to the hydroxyl group of Thr182. However, this network of hydrogen-bonding interactions is disrupted by the replacement of the tyrosine residue that is present in the bacterial ASADHs and is crucial in forming the communication link between the two subunits by a leucine (Leu183; Fig. 5). Either leucine or methionine is found at this position in most fungal ASADHs. This replacement also results in a loss of π-stacking interactions observed across the dimer interface, which is compounded by the replacement of the stabilizing phenylalanine residues that flank the tyrosines in *vc*ASADH and in nearly all of the fungal ASADHs by a valine (Val338). These replacements effectively interrupt the intersubunit-communication channel that links the active sites in the bacterial ASADH dimers. Similar disruption of intersubunit communication is observed in the archaeal ASADH from *M. jannaschii*, in which the critical tyrosyl residue is replaced by a methionine and the phenylalanyl residue by a threonine (Faehnle *et al.*, 2005).

Previous comparisons among members of the ASADH enzyme family also showed a correlation between the overall extent of surface contacts between the subunits at the dimer interface and enzyme activity. The enzyme orthologs with the smallest buried dimer surface and the smallest percentage of buried surface area were found to have the lowest k_{cat} values (Viola *et al.*, 2008). When this new *ca*ASADH structure is compared with these other enzymes it has the lowest subunit surface area ($\sim$1800 Å^2) and the lowest percentage buried surface area (11%), which are consistent with its very low catalytic activity.

3.7. Structure–activity relationships

While the residues in the active site are highly conserved throughout the ASADH family, the catalytic activity of this fungal ortholog is much lower than those of other ASADHs that have been kinetically characterized. The k_{cat} of this fungal enzyme is only 0.12 ± 0.01 s^{-1}, which is more than three orders of magnitude lower than the most active ASADHs. The Gram-negative forms of this enzyme have k_{cat} values ranging from 610 s^{-1} for the *E. coli* enzyme to 58 s^{-1} for the enzyme from *V. cholera* (Moore *et al.*, 2002), while the Gram-positive enzyme from *S. pneumonia* has a k_{cat} value of 2 s^{-1} (Faehnle *et al.*, 2006). A comparison of the structure of the fungal enzyme with those of the other ASADHs provides some insights into how the catalytic activities of these related enzymes can be affected by subtle differences in structural features. While the identity of the catalytic and substrate-binding groups are fully conserved, the catalytic cysteine in *ca*ASADH is found to exist partially in a nonproductive alternative conformation (Fig. 3). Since neither ASA nor an amino-acid analog are present in this complex it is possible that the equilibrium between the productive and nonproductive orientations of the active-site nucleophile could be altered upon substrate binding. It is therefore unclear whether any fraction of the enzyme nucleophile will remain in this nonproductive conformation during the catalytic cycle, thereby contributing to the lower activity of this fungal ASADH.

The orientation of the ASA substrate-binding groups are essentially unchanged between *ca*ASADH and the other members of this enzyme family (Fig. 3), so it is unlikely that the lower activity of the fungal ortholog is a consequence of changes in how this enzyme binds its amino-acid substrate. However, there are substantial differences in how *ca*ASADH binds its coenzyme substrate. The missing β-strand in the third β-α-β motif of the *ca*ASADH structure is similar to what was observed with *mj*ASADH and the absence of this β-strand has been reported to affect coenzyme binding and contribute to the lower enzymatic activity found in the archaeal ortholog (Faehnle *et al.*, 2005). The archaeal ASADH also lacks well defined density for the nicotinamide moiety of the bound NADP, similar to what is seen for this fungal ASADH. This conformational flexibility in the portion of the cofactor that accepts the hydride from the substrate could be a contributing factor to the lower catalytic efficiency.

The loss of intersubunit communication in this fungal ortholog of ASADH is also proposed to play a role in its low catalytic activity. The helical subdomain in the bacterial forms

of ASADH that provides contacts between the dimerization domain of one subunit and the coenzyme-binding domain of the adjacent subunit is absent in the *ca*ASADH structure. In addition, the hydrogen-bonding network that connects the two active sites in *vc*ASADH and *sp*ASADH is missing in *ca*ASADH. The low-activity archaeal ASADH also lacks these intersubunit-communication channels that are present in bacterial ASADHs. Firstly, the helical subdomain is truncated in the archaeal enzymes and can no longer make contact across the dimer interface. Also, the hydrogen-bonding network that provides a link between the active sites in the bacterial enzymes is interrupted in *mj*ASADH, with conserved methionines replacing the bridging tyrosines and the stabilizing aromatic phenylalanines replaced by threonines (Faehnle *et al.*, 2005). As a consequence, the alternating-site reactivity that is seen in bacterial ASADHs (Biellmann *et al.*, 1980) is likely to be absent in both the fungal and archaeal forms of ASADH. Requiring the catalytic cycle in adjacent subunits to function out of phase (alternating-site reactivity) would not appear to offer a catalytic advantage when compared with each site functioning independently. However, if the protein motions that are involved in substrate binding in one subunit can be coupled to complementary motions needed for product release in the adjacent subunit then an energetic advantage can be achieved. These types of coupled motions have been identified in a detailed analysis of the catalytic cycle of ASADH from *E. coli* (Nichols *et al.*, 2004). The loss of this network of hydrogen-bonding interactions in *ca*ASADH as well as the absence of the helical subdomain will clearly affect intersubunit communication, requiring each subunit to function as an isolated catalytic entity and being likely to contribute to the lower catalytic efficiency of the fungal ASADHs.

4. Conclusions

The first structure of a fungal ortholog of ASADH has a similar overall fold and domain organization to the other members of this enzyme family. However, differences in the positioning of the active-site nucleophile, the orientation of the nucleotide cofactor and the nature of the subunit interface in the functional dimer are proposed to contribute to the lower catalytic efficiency of *C. albicans* ASADH.

Use of the Argonne National Laboratory at the Advanced Photon Source was supported by US Department of Energy, Office of Energy Research under Contract No. W-31-109-ENG-38. We thank the staff members at the GM/CA beamline for their assistance with data collection.

References

Biellmann, J. F., Eid, P. & Hirth, C. (1980). *Eur. J. Biochem.* **104**, 59–64.
Blanco, J., Moore, R. A., Kalabeeswaran, V. & Viola, R. E. (2003). *Protein Sci.* **12**, 27–33.
Cohen, G. N. (1985). *Methods Enzymol.* **113**, 596–599.
Collaborative Computational Project, Number 4 (1994). *Acta Cryst.* D**50**, 760–763.
Emsley, P. & Cowtan, K. (2004). *Acta Cryst.* D**60**, 2126–2132.
Faehnle, C. R., Liu, X., Le Coq, J. & Viola, R. E. (2006). *J. Biol. Chem.* **281**, 31031–31040.
Faehnle, C. R., Ohren, J. F. & Viola, R. E. (2005). *J. Mol. Biol.* **353**, 1055–1068.
Gerdes, S. Y. *et al.* (2003). *J. Bacteriol.* **185**, 5673–5684.
Hadfield, A. T., Shammas, C., Kryger, G., Ringe, D., Petsko, G. A., Ouyang, J. & Viola, R. E. (2001). *Biochemistry*, **40**, 14475–14483.
Heijenoort, J. van (2001). *Nat. Prod. Rep.* **18**, 503–519.
Karsten, W. E. & Viola, R. E. (1991). *Biochim. Biophys. Acta*, **1077**, 209–219.
Kobayashi, K. *et al.* (2003). *Proc. Natl Acad. Sci. USA*, **100**, 4678–4683.
Lyon, G. J. & Novick, R. P. (2004). *Peptides*, **25**, 1389–1403.
McCoy, A. J., Grosse-Kunstleve, R. W., Storoni, L. C. & Read, R. J. (2005). *Acta Cryst.* D**61**, 458–464.
Moore, R. A., Bocik, W. E. & Viola, R. E. (2002). *Protein Expr. Purif.* **25**, 189–194.
Nichols, C. E., Dhaliwal, B., Lockyer, M., Hawkins, A. R. & Stammers, D. K. (2004). *J. Mol. Biol.* **341**, 797–806.
Otwinowski, Z. & Minor, W. (1997). *Methods Enzymol.* **276**, 307–326.
Ragkousi, K., Eichenberger, P., van Ooij, C. & Setlow, P. (2003). *J. Bacteriol.* **185**, 2315–2329.
Thanassi, J. A., Hartman-Neumann, S. L., Dougherty, T. J., Dougherty, B. A. & Pucci, M. J. (2002). *Nucleic Acids Res.* **30**, 3152–3162.
Viola, R. E. (2001). *Acc. Chem. Res.* **34**, 339–349.
Viola, R. E., Liu, X., Ohren, J. F. & Faehnle, C. R. (2008). *Acta Cryst.* D**64**, 321–330.
Winn, M. D., Isupov, M. N. & Murshudov, G. N. (2001). *Acta Cryst.* D**57**, 122–133.